Wind and Structures, Vol. 12, No. 3 (2009) 239-257
DOI: http://dx.doi.org/10.12989/was.2009.12.3.239

POD-based representation of the alongwind Equivalent Static Force for long-span bridges

Alessandra Fiore* and Pietro Monaco

Politecnico di Bari, Department of Civil and Environmental Engineering, Via Orabona 4, 70125 Bari, Italy
(Received March 11, 2008, Accepted March 16, 2009)

Abstract. This paper develops and discusses a method by which it is possible to evaluate the Equivalent Static Force (ESF) of wind in the case of long-span bridges. Attention is focused on the alongwind direction. The study herein carried out deals with the classical problems of determining the maximum effects due to the alongwind action and the corresponding ESFs. The mean value of the maximum alongwind displacement of the deck is firstly obtained both by the spectral analysis and the Gust Response Factor (GRF) technique. Successively, in order to derive the other wind-induced effects acting on the deck, the Gust Effect Factor (GEF) technique is extended to long-span bridges. By adopting the GRF technique, it is possible to define the ESF that applied on the structure produces the maximum alongwind displacement. Nevertheless the application of the ESF so obtained does not furnish the correct maximum values of other wind-induced effects acting on the deck such as bending moments or shears. Based on this observation, a new technique is proposed which allows to define an ESF able to simultaneously reproduce the maximum alongwind effects of the bridge deck. The proposed technique is based on the GEF and the POD techniques and represents a valid instrument of research for the understanding of the wind excitation mechanism.

Keywords: Long-span bridge; alongwind effects; Proper Orthogonal Decomposition; Gust Effect Factor technique; Equivalent Static Force.

I. Introduction

The codes in force and in particular Eurocode 1 (UNI EN 1991-1-4 2005) do not furnish any indication in order to calculate the Equivalent Static Force (ESF) of wind in the case of long-span bridges, such as suspension and cable-stayed bridges.

The ESF of wind should represent the force able to reproduce all the maximum load-effects of the deck. In this way engineering calculation may be carried out applying on the structure only one static load.

The first methods aimed at determining an ESF able to simultaneously reproduce the maximum effects due to the wind action have been pioneered in recent years with regard to large-span roofs and vertical structures. More precisely Katsumura, *et al.* (2005) proposed a universal Equivalent Static Wind Load (ESWL), expressed by a combination of eigenmodes, simultaneously reproducing maximum load effects on large-span cantilevered roofs. Repetto and Solari (2004), with reference to

* Corresponding Author, E-mail: a.fiore@poliba.it

vertical structures, developed the Global Loading (GL) technique defining a unique loading condition able to furnish, for each motion direction, all maximum load effects. The GL technique is based on the Influence Function Technique (IFT) and expresses the ESF through a polynomial expansion. It is proposed in two different versions: one is based on the application of the Gust Factor (GF) technique and is denoted by GL/1; the other is used within the framework of the Load Combination (LC) technique and is denoted by GL/2.

In this paper attention is focused on the GL technique. Differently from vertical structures, the GL technique does not furnish correct results in the case of long-span bridges; this is due to the orthogonality properties between power functions and the influence lines of wind-induced effects such as displacements, bending moments or shears, that is bridge influence lines and power functions have not similar shapes.

Thus, in order to define a load distribution suitable for long-span bridges and able to estimate simultaneously the maximum alongwind effects of the deck, a modified GL/1 technique is proposed. It consists in expressing the ESF through a linear combination of spectral or covariance eigenfunctions. Spectral and covariance eigenfunctions are derived by the Proper Orthogonal Decomposition (POD) of the wind velocity field, which is decomposed in a summation of fully coherent terms, statistically uncorrelated, referred to as the modes of the loading process. POD is called Spectral Proper Transformation (SPT) or Covariance Proper Transformation (CPT) according to whether the loading components are the eigenfunctions of the cross power spectral density function (cpsdf) or of the covariance function of the process.

Thanks to the use of POD the problem considerably simplifies and assumes noteworthy analytical and conceptual properties. In fact a limited number of loading modes is enough to express the ESF simultaneously reproducing the maximum alongwind effects of the deck. Moreover the proposed method allows a physical interpretation of the wind excitation mechanism; it particularly enables to quantify the capacity of the single wind modes to dynamically excite the structure.

2. Modeling of the wind field

Let us consider a bridge deck immersed in a turbulent wind field. Let x, y, z be a Cartesian reference system with the x and the z axes belonging to a horizontal plane, z being parallel to the bridge deck axis; the y axis is vertical.

This section deals with the longitudinal component of the wind action. The wind velocity is schematised as the sum of a mean value, function of the position, and of a zero mean stationary fluctuation, function of the position and of the time. For the sake of simplicity, the representation of the wind field is here simplified introducing the following hypotheses: the mean wind velocity is orthogonal to the bridge deck axis; the longitudinal turbulence component is uncorrelated with the lateral and vertical components; the contribution of the vertical turbulence component is neglected; wind actions are applied only to the bridge deck.

The mean wind velocity $\bar{u}$ is expressed by the logarithmic law (Solari and Piccardo 2001). Under the hypothesis of homogeneous and level ground, the mean wind velocity at the height of the deck is constant.

The longitudinal turbulence component is expressed as the product of the standard deviation σ_u and the reduced turbulence $u'(z, t)$, characterized by unit variance. The complete statistical representation of the reduced turbulence is provided by its cpsdf $S_u(z, z', \omega)$, given by:

$$S_u(z, z', \omega) = \overline{S_u}(\omega)\mathrm{Coh}_u(z, z', \omega); \quad \mathrm{Coh}_u(z, z', \omega) = \mathrm{e}^{-\frac{C_{uz}|z-z'|}{2\pi\bar{u}(h)}\cdot|\omega|};$$
$$\overline{S_u}(\omega) = \frac{0.546 \cdot L_u(h)/\bar{u}(h)}{\left[1 + \frac{3 \cdot 0.546 \cdot L_u(h)}{\bar{u}(h)}|\omega|\right]^{5/3}}; \tag{1}$$

where ω is the circular frequency; h is the height of the bridge deck; C_{uz} and $L_u(h)$ are respectively the exponential decay factor and the integral length scale of turbulence (Solari and Piccardo 2001).

The eigenfunctions $\theta_k(z,\omega)$ and the eigenvalues $\gamma_k(\omega)$ of the cpsdf $S_u(z, z', \omega)$ are expressed in the form proposed by Carassale and Solari (2002):

$$\theta_k(z, \omega) = \overline{A_k}(\alpha)\sin\left[\frac{(k\pi - 2\varepsilon_k(\alpha))}{L_T}z + \varepsilon_k(\alpha)\right]; \ \gamma_k(\omega) = \overline{S_u}(\omega)\frac{2}{\alpha}\cos^2[\varepsilon_k(\alpha)]; \ (k = 1,...,N_s); \tag{2}$$

with:

$$\alpha = \frac{C_{uz}L_T}{2\pi\bar{u}(h)}|\omega|; \quad \varepsilon_k(\alpha) = \arctan\left[\frac{\mu_k(\alpha)}{\alpha}\right]; \quad 2\cot(\mu_k) = \frac{\mu_k}{\alpha} - \frac{\alpha}{\mu_k};$$
$$\overline{A_k}(\alpha) = \sqrt{\frac{2(k\pi - 2\varepsilon_k)}{\sin(2\varepsilon_k) + k\pi - 2\varepsilon_k}}; \tag{3}$$

where N_s is the number of significant terms and L_T is the overall length of the deck.

The covariance function can be approximated by the formula (Carassale, *et al*. 1999):

$$C_v(z, z') = e^{-\beta\sqrt{\delta|z-z'|/L_T}}; \quad \delta = \frac{L_T C_{uz}}{L_u(h)}; \quad \beta \cong 0.38[L_u(h)/\bar{u}(h)]^{-0.52}. \tag{4}$$

The covariance eigenfunctions ϕ_k are furnished by:

$$\phi_1 = \frac{1}{\sqrt{2}}; \quad \phi_{k,1}(z) = \sin[2(k-1)\pi z/L_T]; \quad \phi_{k,2}(z) = \cos[2(k-1)\pi z/L_T]; \quad (k = 2,3,...). \tag{5}$$

The whole set of the eigenfunctions $\theta_k(z,\omega)$ and the eigenvalues $\gamma_k(\omega)$ of the cpsdf $S_u(z, z', \omega)$ allows the SPT of the wind velocity field $u'(z, t)$ (Carassale 2005, Carassale, *et al.* 2007, Di Paola and Gullo 2001). That is, applying the POD in the form of a SPT, the reduced turbulence $u'(z, t)$ and the cpsdf $S_u(z, z', \omega)$ assume the form:

$$u'(z, t) = \sum_{k=1}^{N_s}\int_{-\infty}^{+\infty}\mathrm{e}^{\mathrm{i}\omega t}\theta_k(z, \omega)\sqrt{\gamma_k(\omega)\mathrm{d}\omega}W_k(\omega); \quad S_u(z, z', \omega) = \sum_{k=1}^{N_s}\theta_k(z, \omega)\theta_k^*(z', \omega)\gamma_k(\omega); \tag{6}$$

where the asterisk denotes the complex conjugate, i is the imaginary unit and W_k $(k = 1,...,N_s)$ are uncorrelated complex-valued white noises with zero mean and unit variance.

3. Alongwind response by Gust Factor Technique

3.1. Alongwind displacement

Dealing with the bridge as a linear mono-dimensional system, the alongwind displacement of the deck can be expressed in terms of normal modes of vibrations as follows:

$$x(z,t) = \sum_{i=1}^{N_t} \varphi_{xi}(z) p_{xi}(t) \tag{7}$$

where $\varphi_{xi}(z)$ are the structural eigenfunctions; $p_{xi}(t)$ are the principal coordinates; N_t is the number of the structural modes significant for the evaluation of the response. Separating the mean value $\bar{x}(z)$ and the zero-mean fluctuation $x'(z,t)$ of the displacement $x(z,t)$, Eq. (7) can be rewritten as:

$$x(z,t) = \bar{x}(z) + x'(z,t) = \sum_{i=1}^{N_t} \varphi_{xi}(z)(\bar{p}_{xi} + p'_{xi}(t)) \tag{8}$$

where $\bar{p}_{xi}$ and $p'_{xi}(t)$ are respectively the mean value and the zero-mean fluctuation of the i-th principal coordinate $p_{xi}(t)$. Assuming the structure as classically damped, the equation of motion of the deck can be projected in the principal space, obtaining infinite uncoupled equations in terms of principal coordinates. Considering both the mean value $\bar{p}_{xi}$ and the fluctuation $p'_{xi}(t)$, the following equations are obtained:

$$\bar{p}_{xi} = \frac{1}{m_{xi}\omega_{xi}^2} \int_0^{L_T} \bar{F}_x \varphi_{xi}(z)\mathrm{d}z \quad (i = 1,...,N_t) \tag{9}$$

$$\ddot{p}'_{xi}(t) + 2(\tilde{\xi}_{xi} + \tilde{\xi}_{xi}^{o})\omega_{xi}\dot{p}'_{xi}(t) + \omega_{xi}^2 p'_{xi}(t) = \frac{1}{m_{xi}} \int_0^{L_T} F_x'(z,t)\varphi_{xi}(z)\mathrm{d}z \quad (i = 1,...,N_t) \tag{10}$$

where the dot $\cdot$ denotes the derivative with respect to time t; ω_{xi}, m_{xi}, $\tilde{\xi}_{xi}$ and $\tilde{\xi}_{xi}^{o}$ are respectively the alongwind natural circular frequency, the modal mass, the damping ratio and the aerodynamic damping coefficient of the i-th mode; $\bar{F}_x$ and $F_x'(z,t)$ are respectively the mean and buffeting alongwind forces.

Using a linearised quasi-steady approach, under the assumptions introduced in Section 2, the wind forces $\bar{F}_x$ and $F_x'(z,t)$ can be expressed as:

$$\bar{F}_x = \frac{1}{2}\rho \bar{u}^2 B c_D \tag{11}$$

$$F_x'(z,t) = \rho \bar{u}\, \sigma_u u'(z,t) B c_D \tag{12}$$

where $\bar{u} = \bar{u}(h)$; ρ is the air density; c_D is the aerodynamic drag coefficient; B is the deck width.

The quasi-steady theory is substantially reliable since the alongwind response is generally little influenced by vortex shedding (Simiu and Scanlan 1996).

The aerodynamic damping coefficient $\tilde{\xi}_{xi}^{o}$, representing the contribution that the self-excited force

adds to the damping of the deck, and the term m_{xi} are respectively given by:

$$\tilde{\xi}_{xi}^{o} = \frac{1}{m_{xi}} \int_0^{L_T} \frac{\rho \bar{u} B c_D}{2 \omega_{xi}} [\varphi_{xi}(z)]^2 \mathrm{d}z; \quad m_{xi} = \int_0^{L_T} m_x(z) \varphi_{xi}^2(z) \mathrm{d}z. \tag{13}$$

Expressing $u'(z, t)$ and $p'_{xi}(t)$ through the Fourier-Stieltjes integral (Priestley 1981) and considering together Eqs. (8) and (10), the following expression of the power spectral density function (psdf) of $x'(z, t)$ is obtained:

$$S_{xx}(z, \omega) = \sum_{i=1}^{N_t} \sum_{j=1}^{N_t} \varphi_{xi}(z) \varphi_{xj}(z) S_{p_{xi}p_{xj}}(\omega) \tag{14}$$

where $S_{p_{xi}p_{xj}}(\omega)$ is the cpsdf of the principal coordinates $p'_{xi}(t)$ and $p'_{xj}(t)$.

The Gust Response Factor (GRF) technique is an approximate method based on the spectral analysis.

According to the spectral analysis (Davenport 1964), in order to evaluate the mean maximum alongwind displacements in absolute value of the bridge deck, the following expressions are introduced:

$$\begin{cases} \bar{x}_{\max}(z) = \bar{x}(z) + g_x(z) \sigma_x(z) & \bar{x}(z) \geq 0; \\ \bar{x}_{\max}(z) = \bar{x}(z) - g_x(z) \sigma_x(z) & \bar{x}(z) < 0; \end{cases} \tag{15}$$

where $g_x(z)$ and $\sigma_x(z)$ are respectively the peak factor and the root mean square (rms) value of the process $x'(z, t)$ (Solari 1982).

Applying the SPT to the wind velocity field, the cpsdf $S_{p_{xi}p_{xj}}(\omega)$ can be written as:

$$S_{p_{xi}p_{xj}}(\omega) = H_{xi}(\omega) H_{xj}^{*}(\omega) \sum_{k=1}^{N_s} D_{ik}(\omega) D_{jk}^{*}(\omega) \gamma_k(\omega) \quad (i, j = 1,...,N_t) \tag{16}$$

where $D_{ik}(\omega)$ is the i,k-th cross-modal participation coefficient, given by:

$$D_{ik}(\omega) = \int_0^{L_T} \rho \bar{u} \sigma_u B c_D \varphi_{xi}(z) \theta_k(z, \omega) \mathrm{d}z. \tag{17}$$

Eq. (16) derives from the joint application of the modal analysis and of the POD and is therefore the result of the Double Modal Transformation (DMT) technique (Carassale, *et al.* 2001, Solari and Carassale 2000, Solari and Tubino 2005, Tubino and Solari 2007). The generic coefficient $D_{ik}(\omega)$ quantifies the influence of the k-th loading spectral mode on the i-th structural mode of the bridge.

The GRF technique (Davenport 1967) is based on the hypothesis that the structural response is principally given by the first mode of vibration and the contribution of the other modes of vibration is negligible. It consists in expressing the maximum displacement $\bar{x}_{\max}(z)$ as follows:

$$\bar{x}_{\max}(z) = G_x \bar{x}(z) \tag{18}$$

where G_x is the GRF, given by:

$$G_x = 1 + g_x \frac{\sqrt{[\sigma_{Qx}(z)]^2 + [\sigma_{Dx}(z)]^2}}{|\bar{x}(z)|} \tag{19}$$

$\sigma_{Qx}(z)$ and $\sigma_{Dx}(z)$ being respectively the rms values of the quasi-static and resonant parts of $x'(z, t)$. The terms g_x and $\bar{x}(z)$ are evaluated with $N_t = 1$. If the harmonic content of the process $u'(z, t)$ rapidly decreases as the circular frequency increases and the structural damping ratio is ≤ 1, for the rms values $\sigma_{Qx}(z)$ and $\sigma_{Dx}(z)$ the following expressions can be derived:

$$[\sigma_{Qx}(z)]^2 = \frac{2\varphi_{x1}^2(z)}{m_{x1}^2 \omega_{x1}^4} \int_0^{\omega_{x1}} \int_0^{L_T} \int_0^{L_T} S_{Fx}(\zeta, \zeta', \omega) \varphi_{x1}(\zeta) \varphi_{x1}(\zeta') \mathrm{d}\zeta \mathrm{d}\zeta' \mathrm{d}\omega \tag{20}$$

$$[\sigma_{Dx}(z)]^2 = \frac{\pi \varphi_{x1}^2(z)}{2m_{x1}^2 \omega_{x1}^3 (\tilde{\xi}_{x1} + \tilde{\xi}_{x1}^{\rho})} \int_0^{L_T} \int_0^{L_T} S_{Fx}(\zeta, \zeta', \omega_{x1}) \varphi_{x1}(\zeta) \varphi_{x1}(\zeta') \mathrm{d}\zeta \mathrm{d}\zeta' \tag{21}$$

$S_{Fx}(\zeta, \zeta', \omega)$ being the cpsdf of $F_x'(z, t)$. The GRF technique allows also to calculate the ESF $F_{x, eq}$, that is the force distribution that statically applied on the structure produces the maximum alongwind displacement $\bar{x}_{\max}(z)$:

$$F_{x, eq} = \bar{F}_x G_x . \tag{22}$$

Since the GRF technique takes into account only the first mode of vibration, it does not furnish effective results in the case of bridges with more spans. Nevertheless it is consistent with the codes in force with regard to the calculation of the ESF of wind, pointing out the lack of valid methods to this purpose.

In fact it is worth noticing that the codes in force and in particular Eurocode 1 (UNI EN 1991-1-4 2005) expressly do not furnish any indication in order to calculate the ESF of wind acting on long-span bridges such as suspension and cable-stayed bridges. Wind actions are only defined for bridges consisting of a single deck with one or more spans. In this case Eurocode 1 introduces a simplified method which can be used only if a dynamic response procedure is not necessary, but it is apparent that this approximation is not acceptable for long-span bridges. In general for structures Eurocode 1 furnishes also a detailed procedure which takes into account the resonance amplification and can be used only if the following conditions apply: the structure corresponds to one of the general shapes referred to as vertical, horizontal (parallel oscillator) and point-like structures; only the alongwind vibration in the fundamental mode is significant and this mode shape has a constant sign. Thus also the detailed procedure loses its efficacy in the case of long-span bridges. Moreover from a direct inspection of the formulation provided by Eurocode 1, it can be deduced that the ESF obtained by the GRF technique (Eq. (22)) represents an extension of the detailed procedure to long-span bridges. Due to the inadequacy of the GRF technique, there finally emerges the necessity of new methods in order to calculate the ESF of wind in the case of long-span bridges.

3.2. Alongwind effects

The maximum alongwind effects $\bar{e}_{x, \max}(r)$ can be calculated by applying the Gust Effect Factor (GEF) technique. This technique has been developed in literature (Piccardo and Solari 2002,

Repetto and Solari 2004) in the case of vertical structures, characterized by load effects with a constant sign and for which it is sufficient to take into account only the first mode of vibration. In the current treatment the GEF technique is extended to long-span bridges for which the above assumptions are not valid; in fact long-span bridges are characterized by crossed loading effects and the contribution of higher vibration modes is not negligible.

Any load effect e at section r due to the wind loading in the x direction is a random stationary Gaussian process, defined as the sum of a mean value $\bar{e}_x$ and of a zero mean stationary fluctuation e_x'.

Any effect e_x under wind action can assume positive or negative values. Therefore the GEF technique is applied considering the maximum and minimum effects in absolute value and the following expressions are introduced:

$$\bar{e}_{x,\max}(r) = \bar{e}_x(r) G^e_{x,\max}(r); \quad G^e_{x,\max}(r) = 1 + g^e_x(r) \frac{\sqrt{[\sigma^e_{Qx}(r)]^2 + [\sigma^e_{Dx}(r)]^2}}{|\bar{e}_x(r)|} \tag{23}$$

$$\bar{e}_{x,\min}(r) = \bar{e}_x(r) G^e_{x,\min}(r); \quad G^e_{x,\min}(r) = 1 - g^e_x(r) \frac{\sqrt{[\sigma^e_{Qx}(r)]^2 + [\sigma^e_{Dx}(r)]^2}}{|\bar{e}_x(r)|} \tag{24}$$

with:

$$\begin{aligned} g^e_x(r) &= \sqrt{2\ln[\nu^e_x(r)T]} + \frac{0.5772}{\sqrt{2\ln[\nu^e_x(r)T]}}; \\ \nu^e_x(r) &= \sqrt{\frac{[\nu^e_{Qx}(r)\sigma^e_{Qx}(r)]^2 + \sum_{k=1}^{N_t} [\omega_{xk}\sigma^e_{Dx,k}(r)/(2\pi)]^2}{[\sigma^e_{Qx}(r)]^2 + [\sigma^e_{Dx}(r)]^2}}; \end{aligned} \tag{25}$$

$$[\nu^e_{Qx}(r)]^2 = \frac{1}{2\pi^2[\sigma^e_{Qx}(r)]^2} \int_0^{\omega_{x1}} \int_0^{L_T} \int_0^{L_T} \omega^2 S_{Fx}(z, z', \omega)\, \eta^e_x(r, z)\, \eta^e_x(r, z')\, \mathrm{d}z\, \mathrm{d}z'\, \mathrm{d}\omega; \tag{26}$$

$$\bar{e}_x(r) = \int_0^{L_T} \bar{F}_x \eta^e_x(r, z)\, \mathrm{d}z; \quad [\sigma^e_{Qx}(r)]^2 = 2 \int_0^{\omega_{x1}} \int_0^{L_T} \int_0^{L_T} S_{Fx}(z, z', \omega)\, \eta^e_x(r, z)\, \eta^e_x(r, z')\, \mathrm{d}z\, \mathrm{d}z'\, \mathrm{d}\omega; \tag{27}$$

$$[\sigma^e_{Dx}(r)]^2 \cong \sum_{k=1}^{N_t} [\sigma^e_{Dx,k}(r)]^2 = \sum_{k=1}^{N_t} \frac{[m^e_{xk}(r)]^2}{[m_{xk}]^2} \frac{\pi\omega_{xk}}{2(\tilde{\xi}_{xk} + \tilde{\xi}^o_{xk})} \int_0^{L_T} \int_0^{L_T} S_{Fx}(z, z', \omega_{xk})\, \varphi_{xk}(z)\, \varphi_{xk}(z')\, \mathrm{d}z\, \mathrm{d}z' \tag{28}$$

where $G^e_{x,\max}(r)$ and $G^e_{x,\min}(r)$ are the GEFs for the load effect e_x due to the wind loading in the x direction; $g^e_x(r)$ is the peak factor of e_x'; $\sigma^e_{Qx}(r)$ and $\sigma^e_{Dx}(r)$ are respectively the rms values of the quasi-static and resonant parts of e_x'; $\nu^e_x(r)$ and $\nu^e_{Qx}(r)$ are respectively the expected frequencies of e_x' and of its quasi-static part; $m^e_{xk}(r)$ is the effect influence mass in the x direction of the k-th structural mode (Piccardo and Solari 2002); T is the duration of wind loading; $\eta^e_x(r, z)$ is the influence function of e_x, that is the value of e_x at the point having abscissa r due to a unit static action in the x direction applied in correspondence of abscissa z. The above expressions have been derived in the hypotheses that the harmonic content of the process $u'(z, t)$ rapidly decreases as the

circular frequency increases, the structural damping ratio is ≤ 1 and the natural frequencies of the bridge are well separated. Focusing on the maximum effects, the ESF that produces the effect $\bar{e}_{x,\max}(r)$ in section r is given by:

$$F^{e}_{x,eq}(r) = G^{e}_{x,\max}(r)\overline{F}_x . \tag{29}$$

The ESF so defined depends on the effect e and the section r considered. In fact, since wind induced responses vary in time and space, the maximum load effects do not occur simultaneously.

Generally in the case of long-span bridges the application of the ESF associated to the maximum displacement ($e = d$) does not furnish the correct maximum values of other wind-induced effects e acting on the deck such as bending moments ($e = b$) or shears ($e = s$), that is in a generic section r $G^{d}_{x,\max}(r) \neq G^{b}_{x,\max}(r)$ and $G^{d}_{x,\max}(r) \neq G^{s}_{x,\max}(r)$. These aspects make the GEF technique unsuitable for engineering applications.

4. Proposed method

In the light of the above considerations, a modified GL/1 technique is proposed which defines a unique ESF able to simultaneously reproduce the maximum alongwind effects of the bridge deck.

It consists in expressing the alongwind ESF through a combination of spectral or covariance eigenfunctions. Adopting spectral eigenfunctions $\theta_k(z, \omega_{x1})$, the ESF is expressed as:

$$F_{x,eq}(z) = \overline{F}_x \sum_{k=1}^{N} c_{xk}\theta_k(z, \omega_{x1}) \tag{30}$$

where c_{xk} (k=1,2,....N) are N coefficients used to impose that Eq. (30) gives rise to the correct values of the N specified load effects and ω_{x1} is the first natural circular frequency of the deck in the x direction.

According to the IFT, in order to produce the N specified maximum effects $\bar{e}_{x,\max}(r)$, the ESF for each of them has to satisfy the following relationship:

$$\overline{F}_x \sum_{k=0}^{N} c_{xk} \int_0^{L_T} \theta_k(z, \omega_{x1})\,\eta^{e}_{x}(r, z)\mathrm{d}z = \bar{e}_{x,\max}(r) . \tag{31}$$

Applying the GEF technique and considering together Eqs. (31) and (23), the following system of N equations in N unknowns c_{xk} is obtained:

$$\overline{F}_x \sum_{k=1}^{N} c_{xk} \int_0^{L_T} \theta_k(z, \omega_{x1})\,\eta^{e}_{x}(r, z)\mathrm{d}z = G^{e}_{x,\max}(r)\overline{F}_x \int_0^{L_T} \eta^{e}_{x}(r, z)\mathrm{d}z . \tag{32}$$

The procedure is analogous if covariance eigenfunctions $\phi_k(z)$ are used in place of spectral modes $\theta_k(z, \omega_{x1})$.

The described method represents a simple procedure for properly simulating the ESF of wind in the case of long-span bridges. Moreover the application of POD suggests a physical interpretation of the wind excitation mechanism; in fact the analysis of the integrals $\int_0^{L_T} \theta_k(z, \omega_{x1})\,\eta^{e}_{x}(r, z)\mathrm{d}z$ ($\int_0^{L_T} \phi_k(z)\,\eta^{e}_{x}(r, z)\mathrm{d}z$)

allows to quantify the capacity of the single wind modes to dynamically excite the structure.

5. Numerical application

The numerical applications deal with the case of a self-anchored cable-stayed bridge with two spans, a curtain suspension, stays disposed fanwise and an A-shaped pylon (Fig. 1).

The linearised equation concerning the motion of the deck in the x direction has been derived by a continuous variational formulation in a non-linear field based on the application of Hamilton's principle and is reported in Appendix. The structural eigenfunctions $\varphi_{xi}(z)$ (i=1,...,N_t) have been obtained by applying the numerical method proposed by Monaco and Fiore (2005). By the application of the orthogonality conditions of the structural eigenfunctions, the equation of motion of the deck has been projected in the principal space, obtaining infinite uncoupled equations in terms of principal coordinates.

With reference to Eqs. (10) and (13), the terms $m_x(z)$ and $\tilde{\xi}_{xi}$ are given by:

$$m_x(z) = \left\{ \frac{2}{3}\frac{\gamma_C}{g} a_C s_C^{(\circ)}(z) \left[1 + \left(\frac{C_V(z)B}{2h_P} \right)^2 \right] + m_T \left[1 + \left(\frac{C_V(z)B^2}{4h_P^2} \right) \right] \right\}; \tag{33}$$

$$\tilde{\xi}_{xi} = \frac{1}{m_{xi}} \int_0^{L_T} \left\{ \xi_C \frac{2}{3}\frac{\gamma_C a_C}{g} s_C^{(\circ)}(z) \left[1 + \left(\frac{C_V(z)B}{2h_P} \right)^2 \right] + \xi_T m_T \left[1 + \left(\frac{C_V(z)B^2}{4h_P^2} \right) \right] \right\} [\varphi_{xi}(z)]^2 \mathrm{d}z; \tag{34}$$

where γ_C is the specific weight of the stays; $s_C^{(\circ)}(z) = \sqrt{(B/2)^2 + h_P^2 + (z - l_1)^2}$ is the length of the generic curtain cable span; a_C is the area per linear metre of the suspension cables; m_T is the mass per length unit of the deck; $C_V(z) = [h_P^2/(h_P^2 + (z - l_1)^2)]$; ξ_C and ξ_T are respectively the damping ratios of the stays and of the deck. Simplified expressions of the functions $C_V(z)$ and $s_C^{(\circ)}(z)$ have been obtained by Monaco and Fiore (2005). From a direct inspection of Eq. (34) it can be noted that the coefficient $\tilde{\xi}_{xi}$ expresses the overall damping of the deck, taking into account also the influence of the stays.

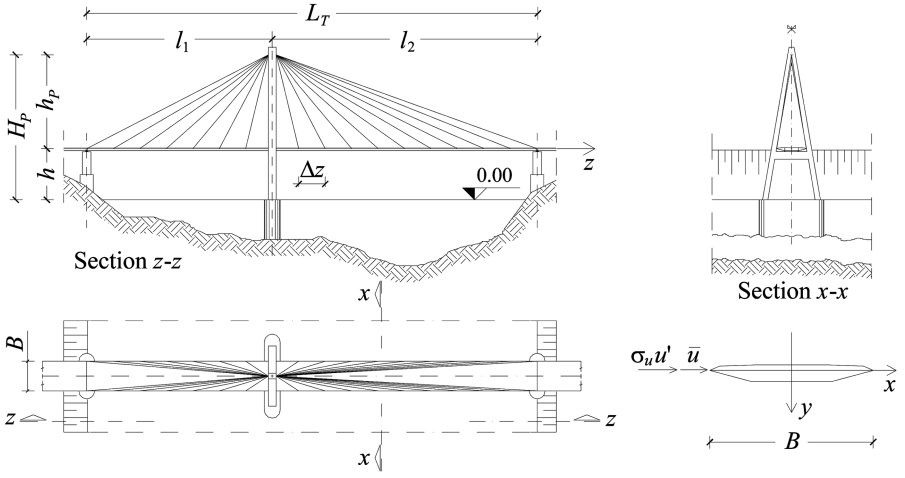

Fig. 1 Cable-stayed bridge under examination

Table 1 provides the geometrical and mechanical data of the bridge. As to the wind action, the following parameters are assumed: $c_D = 0.1$ (Larose and Livesey 1997), $\rho = 1.25$ kg/m^3, y_o=0.01 m, $u_* = 2.38$ m/s, $C_{uz} = 10$, $T = 600$ s, where u_* and y_o are respectively the shear velocity and the roughness length. Thus the mean wind velocity at the height h of the deck is equal to $\bar{u} = 49.41$ m/s. It also results $\sigma_u = 6.46$ m/s and $L_u(h) = 148.48$ m.

Fig. 2 shows the first three structural and spectral eigenfunctions. Fig. 3 provides the cross-modal participation coefficients $D_{1k}(\omega)$ and $D_{2k}(\omega)$ (k=1,...,5). In correspondence of structural and loading eigenfunctions having similar shapes, the cross-modal participation coefficients are much greater than the others.

The alongwind response is firstly evaluated by applying the spectral analysis. Observing Fig. 2, it can be noted that the first and the second structural modes are connected respectively to the maximum displacements of the second and the first span of the bridge; moreover the harmonic content of turbulence rapidly decreases as the circular frequency increases and the natural frequencies of the bridge are well separated.

Therefore the response can be evaluated considering only the contribution of the first two structural

Table 1 Geometrical and mechanical characteristics of the cable-stayed bridge

l_1=147.42 [m]	L_T=358.02 [m]	h_P=74.2 [m]	h=40.4 [m]	B=23.46 [m]	m_T=19.68 [kNs^2/m^2]
g=9.81 [m/s^2]	Δz=21.06 [m]	ξ_C=0.001	ξ_T=0.004	a_C=0.000537 [m^2/m]	γ_C=7.85 10^{-5} [kN/cm^3]

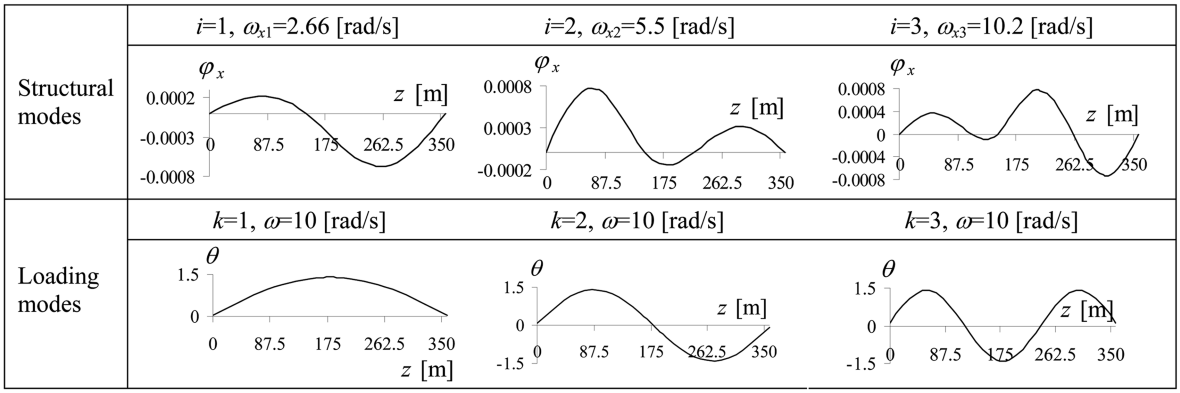

Fig. 2 First three structural and spectral eigenfunctions

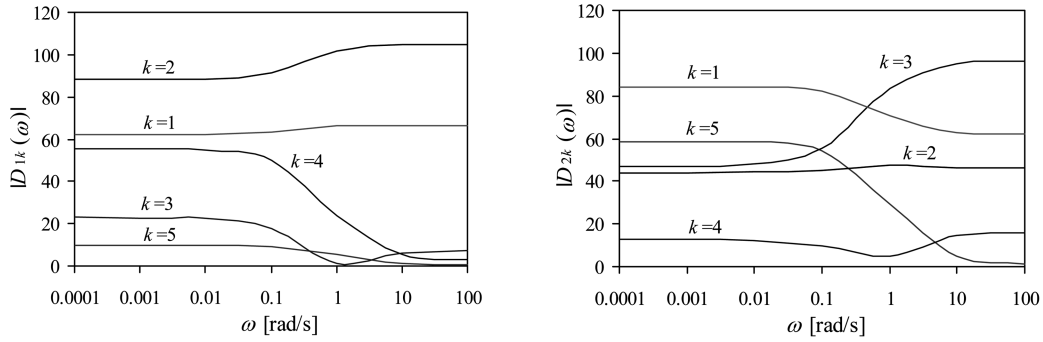

Fig. 3 Cross-modal participation coefficients D_{1k} (k=1,…,5) and D_{2k} (k=1,…,5)

modes ($N_t = 2$) without making a significant mistake. This statement can be easily verified comparing the diagram of mean displacements $\bar{x}(z)$ obtained by Eq. (8) (with $N_t = 2$) with the one calculated by a finite elements structural analysis code (SAP2000) applying on the bridge deck the mean force $\overline{F}_x$.

Fig. 4a shows the psdf $S_{xx}(z, \omega)$ obtained by applying Eqs. (14) and (1) ($N_s = \infty$) and its modal recomposition obtained by introducing Eq. (16), calculated in correspondence of the section $z = 252.72$ m; it can be noted that for $N_s = 5$ the two curves coincide. This remark points out that it is sufficient to take into account only the first five loading modes ($N_s = 5$) for the evaluation of the response. Fig. 4b shows the diagrams of the mean and maximum displacements of the bridge deck obtained by applying respectively Eqs. (8) and (15).

The solutions so obtained are compared with the results of the GRF technique. Fig. 5 provides the diagrams of the mean and maximum displacements of the bridge deck obtained by applying respectively Eqs. (8) (with $N_t = 1$) and (18). Since the GRF technique takes into account only the first mode of vibration, it furnishes correct solutions only for the second span, as it can be noted comparing Figs. 4b and 5. In particular the application of Eq. (18) leads to a maximum alongwind displacement in correspondence of $z = 252.72$ m equal to 6.6 cm (Table 2).

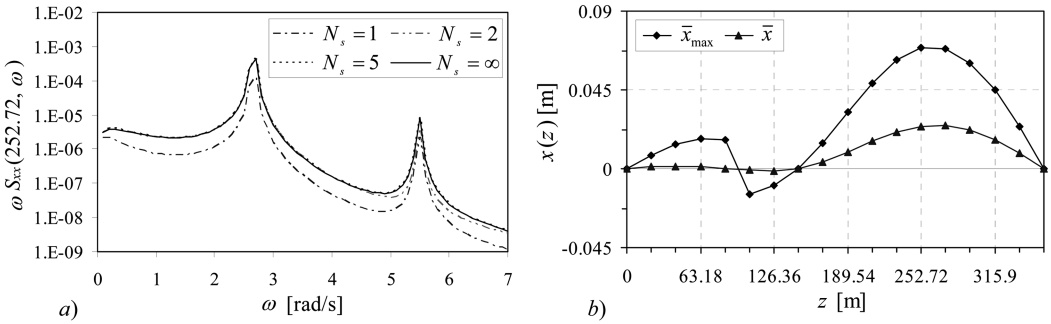

Fig. 4 a) Psdf $S_{xx}(z,\omega)$ in correspondence of $z = 252.72$ (m); b) displacements $\bar{x}(z)$ and $\bar{x}_{max}(z)$ according to the spectral analysis

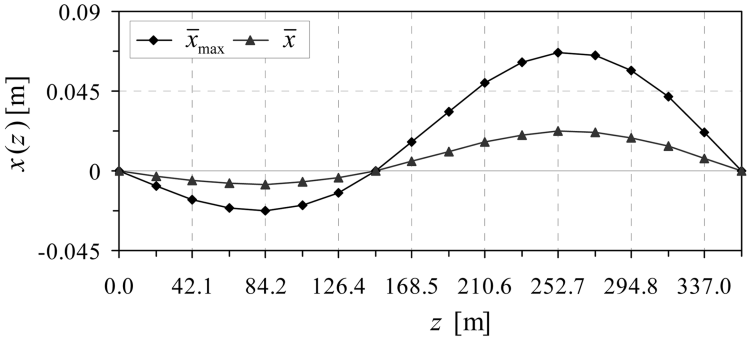

Fig. 5 Displacements $\bar{x}(z)$ and $\bar{x}_{max}(z)$ according to the GRF technique

Table 2 Results obtained by the GRF technique

G_x	ν_x [Hz]	g_x	$\sigma_x(252.72)$ [m]	$\bar{x}(252.72)$ [cm]	$\bar{x}_{max}(252.72)$ [cm]
2.988	0.39	3.478	0.0127	2.2	6.6

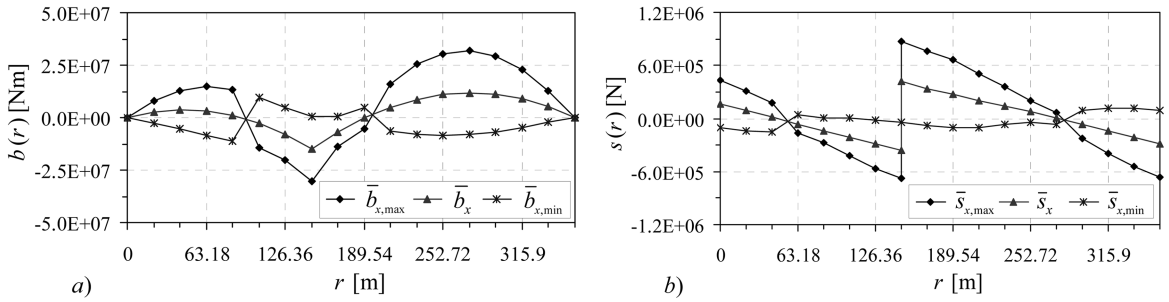

Fig. 6 Diagrams of $\bar{e}_x(r)$, $\bar{e}_{x,\max}(r)$ and $\bar{e}_{x,\min}(r)$: a) $e = b$; b) $e = s$

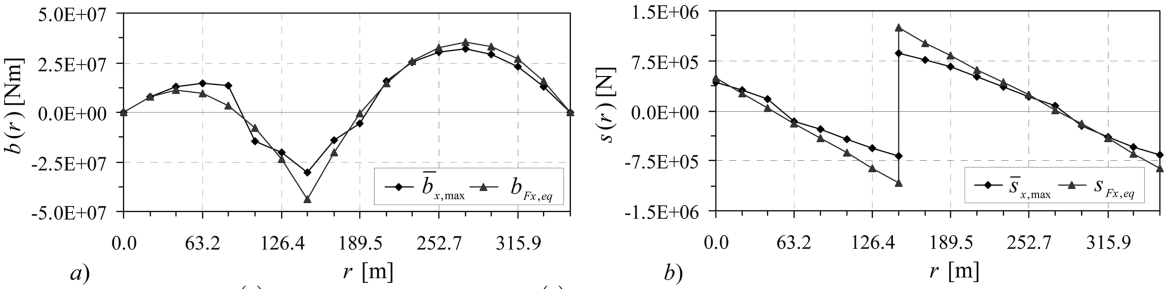

Fig. 7 Diagrams of $\bar{e}_{x,\max}(r)$ and of the load effects $e_{Fx,eq}(r)$ generated by the ESF $F_{x,eq}$ (GRF): a) $e = b$; b) $e = s$

As to the GEF technique, Figs. 6a and 6b show the mean, maximum and minimum values respectively of the bending moments (e=b) and shears (e=s) obtained by applying Eqs. (27), (23) and (24).

Figs. 7a and 7b compare the maximum effects $\bar{b}_{x,\max}(r)$ and $\bar{s}_{x,\max}(r)$ respectively with the bending moments $b_{Fx,eq}$ and shears $s_{Fx,eq}$ produced by the ESF $F_{x,eq}$ calculated by the GRF technique (Eq. (22)), which represents an extension to long-span bridges of the detailed procedure provided by Eurocode 1. It emerges that the application of the ESF associated to the maximum displacement does not furnish the correct maximum values of other wind-induced effects e acting on the deck such as bending moments ($e = b$) or shears ($e = s$). In particular the application of the load distribution $F_{x,eq}$ involves an underestimation of the maximum effects in the first span and an overestimation in correspondence of the pylon.

The proposed method is firstly applied in order to research the load distribution that in a specified section r of the deck simultaneously produces the mean maximum values of the displacement ($e = d$), bending moment ($e = b$) and shear ($e = s$) effects. In this case the system (32) is constituted by $N = 3$ equations in $N = 3$ unknowns c_{xk}. Figs. 8a and 8b show the distributions of the ESF $F_{x,eq}(z)$ simultaneously generating the maximum effects $\bar{e}_{x,\max}(r)$ ($e = d$, b, s) respectively in the sections $r = 147.42_{\mathrm{R}}$ m and r=252.72 m (pedices R and L mean immediately at the right and at the left of the point r=147.42 m); the corresponding coefficients c_{xk} ($k = 1,2,3$) are reported in Table 3. In each of Figs. 8a and 8b also the forces $F^{e}_{x,eq}(r)$ ($e = d$, b, s) that singly produce the corresponding maximum effects $\bar{e}_{x,\max}(r)$ in the considered sections are represented.

Nevertheless the load distributions so obtained, referring to just one specified section, do not provide the correct values of maximum effects in many other sections of the bridge deck.

This remark can be observed in Figs. 9a, b, c, where the diagrams of $\bar{d}_{x,\max}(r)$, $\bar{b}_{x,\max}(r)$ and

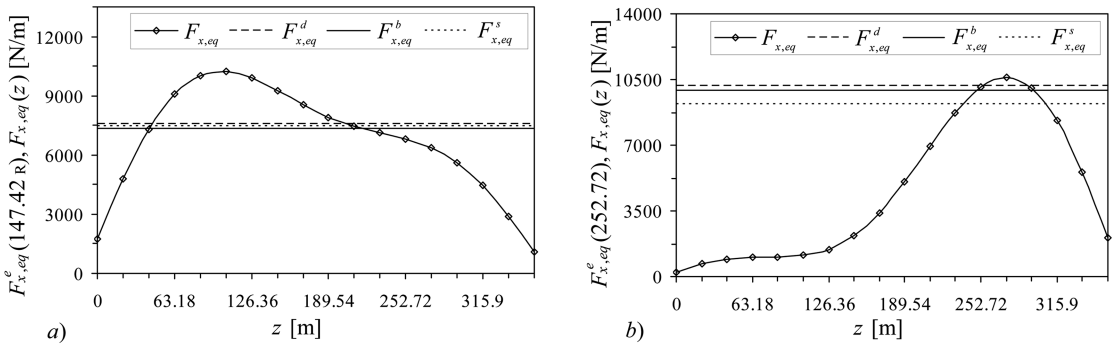

Fig. 8 Diagrams of $F^e_{x,eq}(r)$ (e=d, b, s) and $F_{x,eq}(z)$ in correspondence of the section a) $r = 147.42_R$ (m); b) $r = 252.72$ (m)

Table 3 Coefficients c_{xk} (k=1,2,3)

r [m]	c_{x1}	c_{x2}	c_{x3}
147.42_R	2.014	0.373	0.344
252.72	1.265	-0.974	0.414

$\bar{s}_{x,\max}(r)$ are compared respectively with the diagrams of displacements $d_{F_{x,eq}}(r)$, bending moments $b_{F_{x,eq}}(r)$ and shears $s_{F_{x,eq}}(r)$ generated by the ESF corresponding to the sections $r = 252.72$ m (Fig. 8b).

Thus the method is utilized in order to research a load distribution whose application on the bridge deck produces displacement, bending moment and shear diagrams as close as possible to the diagrams of the maximum values of these effects, represented in Figs. 4b, 6a and 6b.

Using spectral eigenfunctions, $N = 14$ conditions are enough to obtain a good approximation.

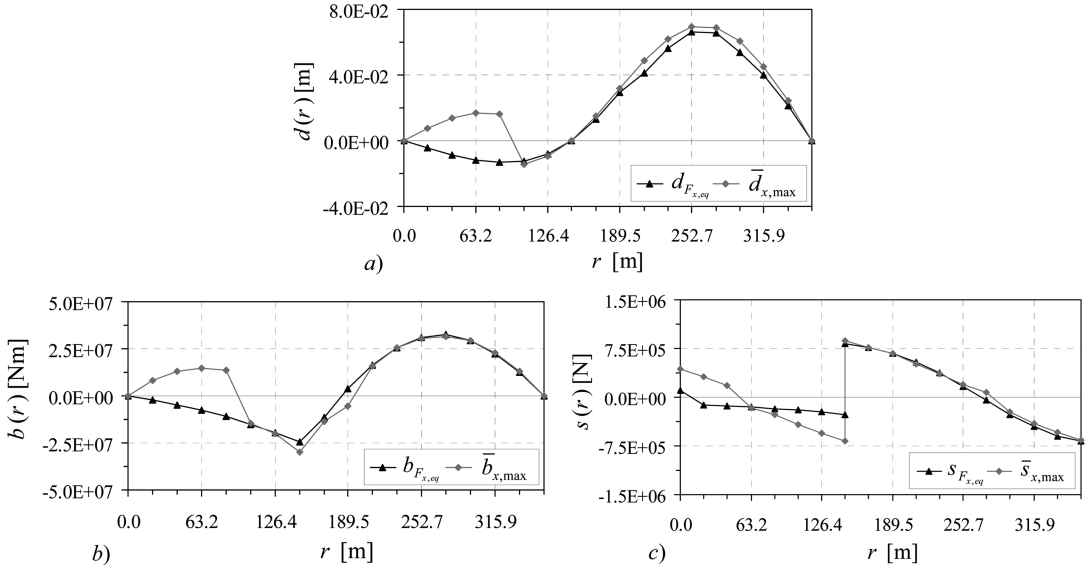

Fig. 9 Diagrams of $\bar{e}_{x,\max}(r)$ and of the load effects $e_{Fx,eq}$ generated by the ESF $F_{x,eq}(z)$ corresponding to the section $r = 252.72$ (m): a) $e = d$; b) $e = b$; c) $e = s$

Considering the following maximum effects:

$$\bar{d}_{x,\max}\ (252.72),\ \bar{b}_{x,\max}\ (21.06),\ \bar{b}_{x,\max}\ (126.36),\ \bar{b}_{x,\max}\ (147.42),\ \bar{b}_{x,\max}\ (189.54),$$
$$\bar{b}_{x,\max}\ (252.72),\ \bar{b}_{x,\max}\ (273.78),\ \bar{s}_{x,\max}\ (0),\ \bar{s}_{x,\max}\ (63.18),\ \bar{s}_{x,\max}\ (147.42_{\mathrm{L}}),$$
$$\bar{s}_{x,\max}\ (147.42_{\mathrm{R}}),\ \bar{s}_{x,\max}\ (252.72),\ \bar{s}_{x,\max}\ (315.9),\ \bar{s}_{x,\max}\ (336.96),$$

the $N = 14$ coefficients c_{xk} ($k = 1,...,14$) calculated by solving the corresponding system assume the values reported in Table 4. Fig. 10a shows the shape of the ESF $F_{x,eq}(z)$ so derived. In Figs. 10b, 10c, and 10d the diagrams of displacements, bending moments and shears generated by the described ESF $F_{x,eq}(z)$ are compared respectively with the diagrams of their maximum values. Figs. 11a, b, c, d show respectively the reconstructions of $F_{x,eq}(z)$, $d_{F_{x,eq}}(r)$, $b_{F_{x,eq}}(r)$ and $s_{F_{x,eq}}(r)$ on increasing the number of loading modes.

Using covariance eigenfunctions ($\phi_{k,1}$), at least $N = 17$ conditions are necessary in order to obtain a satisfactory representation of the ESF. Considering together the 14 effects above listed and the maximum effects $\bar{b}_{x,\max}(42.12)$, $\bar{b}_{x,\max}(294.84)$, $\bar{s}_{x,\max}(189.54)$, the ESF $F_{x,eq}(z)$ assumes the shape reported in Fig. 12a. Figs. 12b, c, d compare the diagrams of displacements, bending moments and shears generated by the ESF so obtained with the diagrams of their maximum values.

It is apparent that spectral eigenfunctions are more effective if compared to covariance eigenfunctions; in fact a smaller number of loading spectral modes is enough for a suitable prediction of the ESF.

Moreover it is worth noticing that the GL technique introduced by Repetto and Solari (2004) for vertical structures does not furnish correct results in the case of long-span bridges. In fact if the ESF is expressed through a polynomial expansion, the problem does not admit convergence solutions. For example Fig. 13a shows the ESF obtained by using power functions and considering the same

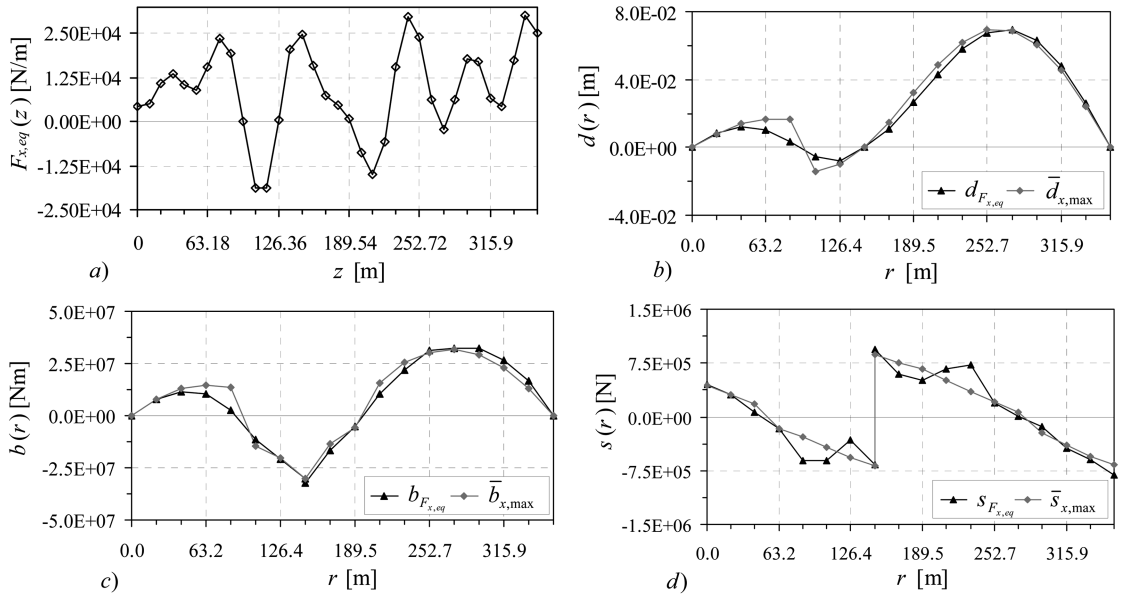

Fig. 10 a) ESF $F_{x,eq}(z)$ obtained by using spectral eigenfunctions and imposing 14 conditions; b-d) diagrams of $\bar{e}_{x,\max}(r)$ and of the load effects $e_{Fx,eq}$ generated by the ESF $F_{x,eq}(z)$: b) $e = d$; c) $e = b$; d) $e = s$

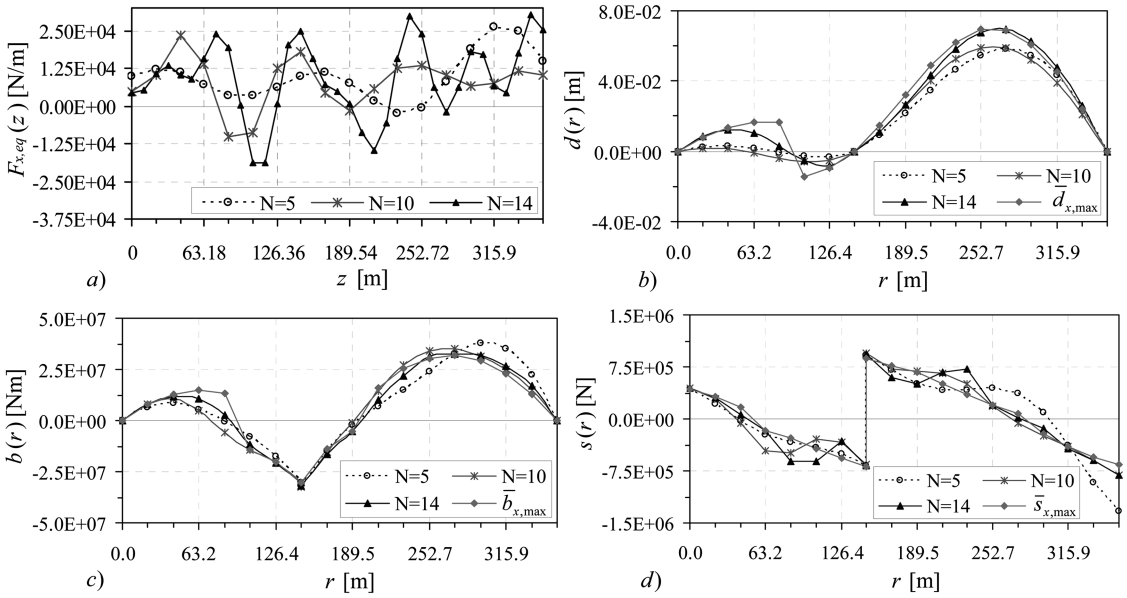

Fig. 11 Reconstruction of: a) the ESF $F_{x,eq}(z)$ obtained by using spectral eigenfunctions and imposing 14 conditions; b) $d_{F_{x,eq}}(r)$; c) $b_{F_{x,eq}}(r)$; d) $s_{F_{x,eq}}(r)$, on increasing the number N of loading modes

Table 4 Coefficients c_{xk} (k=1,...,14)

c_{x1}	c_{x2}	c_{x3}	c_{x4}	c_{x5}	c_{x6}	c_{x7}	c_{x8}	c_{x9}	c_{x10}	c_{x11}	c_{x12}	c_{x13}	c_{x14}
2.06	-0.33	0.95	-0.086	0.48	0.50	0.07	-2.32	-0.097	1.04	0.64	0.046	0.71	-1.93

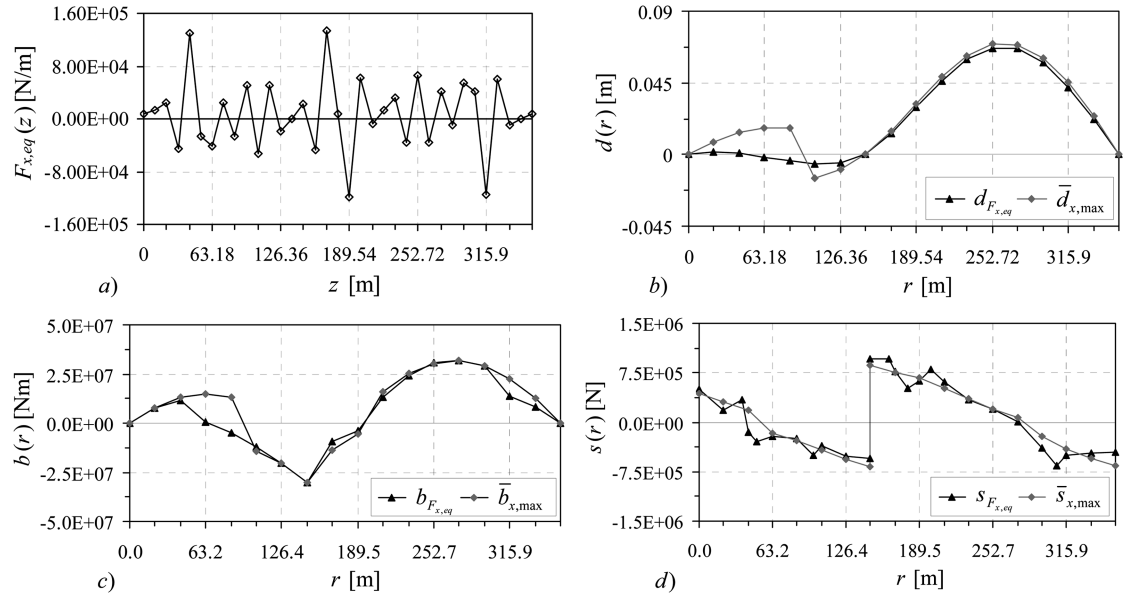

Fig. 12 a) ESF $F_{x,eq}(z)$ obtained by using covariance eigenfunctions and imposing 17 conditions; b-d) diagrams of $\bar{e}_{x,\max}(r)$ and of the load effects $e_{Fx,eq}$ generated by the ESF $F_{x,eq}(z)$: b) $e = d$; c) $e = b$; d) $e = s$

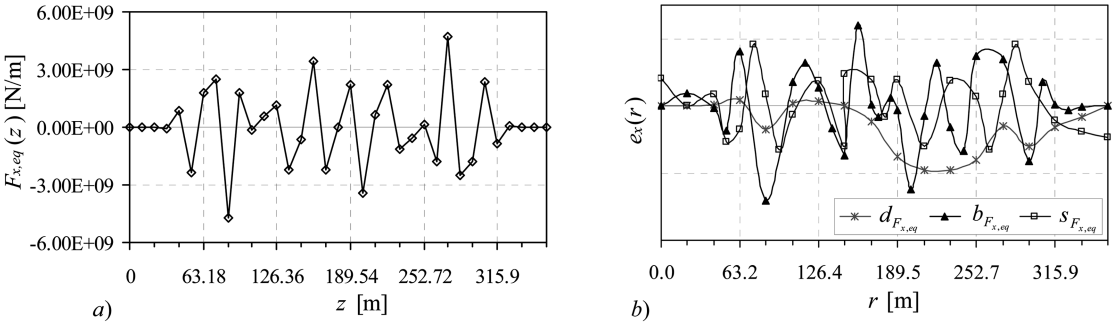

Fig. 13 a) ESF $F_{x,eq}(z)$ obtained by using power functions and imposing 17 conditions; b) shapes of the diagrams of $d_{F_{x,eq}}(r)$, $b_{F_{x,eq}}(r)$ and $s_{F_{x,eq}}(r)$

17 maximum effects adopted in the case of covariance eigenfunctions. The shapes of the corresponding diagrams of displacements, bending moments and shears are reported in Fig. 13b. It emerges the ineffectiveness of this technique in order to simulate the ESF of wind in the case of long-span bridges; this is due to the scarce similarity between power functions and influence lines of loading effects of the bridge deck.

The use of POD enables some formal simplifications and suggests a physical interpretation of the phenomena that produce the external load.

In both cases of spectral and covariance eigenfunctions a small number of POD modes is enough to provide a good representation of the ESF. More precisely it is sufficient to impose a limited number of conditions in order to properly reconstruct the diagrams of maximum displacements, bending moments and shears; that is the ESFs obtained by imposing a limited number of conditions referring to specified significant sections, provide the correct values of maximum effects also in other sections of the bridge deck (Figs. 10, 12). This aspect yields an apparent computational advantage. In particular the numerical application has shown that using spectral eigenfunctions is more effective than adopting covariance modes.

Nevertheless, focusing on spectral eigenfunctions, $N = 14$ POD modes are necessary to reconstruct the alongwind ESF associated simultaneously to maximum displacements, bending moments and shears, while the alongwind response is perfectly estimated with 5 POD modes. This remark demonstrates that more loading modes affect the generalised bending moments and shears with respect to displacements and points out the necessity to take into account simultaneously more loading effects in order to define an effective ESF.

The physical phenomenon can be clarified by analyzing the integrals $\int_0^{L_T} \theta_k(z, \omega_{x1})\, \eta_x^e(r, z)\mathrm{d}z$ ($e = d$, b, s). In fact, while the analysis of the cross-modal participation coefficients enables to quantify the influence of loading modes only on the displacement effect, the analysis of the integrals $\int_0^{L_T} \theta_k(z, \omega_{x1})\, \eta_x^e(r, z)\mathrm{d}z$ allows to quantify at the same time the influence of loading modes on all three of the displacement, bending moment and shear effects. Figs. 14a, b and c show the values of the integrals $\int_0^{L_T} \theta_k(z, \omega_{x1})\, \eta_x^e(r, z)\mathrm{d}z$ ($k = 1,...,15$) respectively in the case of $e = d$, $e = b$ and $e = s$, calculated in correspondence of some

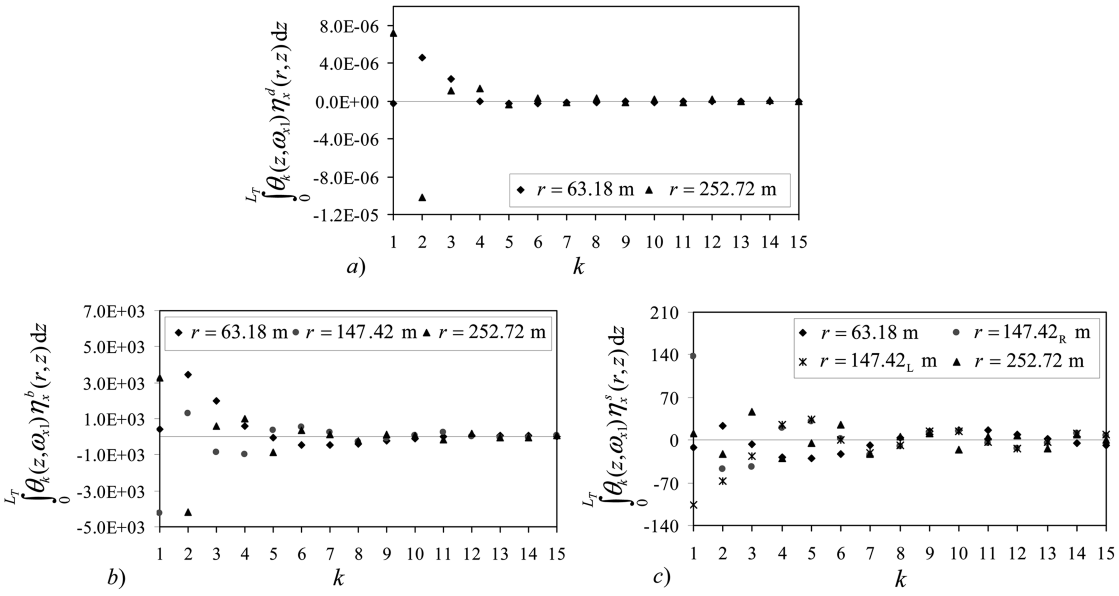

Fig. 14 Integrals $\int_0^{L_T} \theta_k(z, \omega_{x1})\, \eta_x^e(r, z)\mathrm{d}z$ ($k = 1,...,15$): a) $e = d$; b) $e = b$; c) $e = s$

values of r.

It can be noted that for $k > 5$ the values of these integrals are negligible in the first case ($e = d$), while are significant in both the second and third cases ($e = b$; $e = s$). This confirms that, differently from displacements, more loading modes affect bending moments and shears; in particular bending moments and shears are influenced respectively by seven and twelve wind modes.

6. Conclusions

The aim of this paper is defining an ESF of wind suitable for long-span bridges, focusing on the alongwind direction. In fact the codes in force do not furnish any indication about this topic. Moreover the ESF that produces the maximum alongwind displacement generally does not furnish the correct maximum values of other wind-induced effects acting on the deck, such as bending moments and shears.

Based on these considerations, a new method has been proposed which defines an ESF able to simultaneously reproduce the maximum alongwind effects of the deck. The method is based on the GEF and POD techniques and consists in expressing the ESF through a combination of wind modes. The number of loading modes to be considered in defining the ESF is the one allowing to obtain diagrams of the effects under consideration as close as possible to the diagrams of their maximum values. Generally it is sufficient to impose a limited number of conditions referring to significant sections in order to obtain an effective ESF.

The use of POD simplifies the numerical analyses and clarifies the physical phenomenon. In fact, as just discussed, a limited number of loading modes is enough to properly reconstruct the ESF. In addition the introduction of POD allows to quantify the capacity of the single wind modes to dynamically excite the structure. In particular the application of the proposed method has shown that more loading modes affect bending moments and shears with respect to displacements. This remark has demonstrated that a satisfactory representation of the ESF must simultaneously take into account all the significant load effects.

References

Carassale, L., Piccardo, G. and Solari, G. (1999), "Double modal transformation in continuous modeling", *Proc. of the 10th Int. Conf. on Wind Engineering*, Copenaghen.

Carassale, L., Piccardo, G. and Solari, G. (2001), "Double Modal Transformation and Wind Engineering Applications", *J. Eng. Mech. ASCE*, **127**(5), 432-439.

Carassale, L. and Solari, G. (2002), "Wind modes for structural dynamics: a continuous approach", *Probabilistic Eng. Mech.*, **17**, 157-166.

Carassale, L. (2005), "POD-based filters for the representation of random loads on structures", *Probabilistic Eng. Mech.*, **20**, 263-280.

Carassale, L., Solari, G. and Tubino, F. (2007), "Proper Orthogonal Decomposition in wind engineering. Part 2: Theoretical aspects and some applications", *Wind Struct.*, **10**(2), 177-208.

Davenport, A.G. (1964), "Note on the distribution of the largest value of a random function with application to gust loading", *Proc. Inst. Civ. Eng.*, London, **24**, 187-196.

Davenport, A.G. (1967), "Gust loading factors", *J. Struct. Div. ASCE*, **93**, 11-34.

Di Paola, M. and Gullo, I. (2001), "Digital generation of multivariate wind field processes", *Probabilistic Eng. Mech.*, **16**, 1-10.

Katsumura, A., Tamura, Y. and Nakamura, O. (2005), "Universal wind load distribution simultaneously reproducing maximum load effects in all subject members on large-span cantilevered roof", *Proc. of the Fourth European & African Conf. on Wind Engineering*, Prague, July.

Larose, G.L. and Livesey, F.M. (1997), "Performance of streamlined bridge decks in relation to the aerodynamics of a flat plate", *J. Wind Eng. Ind. Aerod.*, **69-71**, 851-860.

Monaco, P. and Fiore, A. (2005), "A method to evaluate the frequencies of free transversal vibrations in self-anchored cable-stayed bridges", *Comput. Concrete*, **2**(2), 125-146.

Piccardo, G. and Solari, G. (2002), "3-D gust effect factor for slender vertical structures", *Probabilistic Eng. Mech.*, **17**, 143-155.

Priestley, M.B. (1981), *Spectral analysis and time series*, London, Academic Press, 1981.

Repetto, M.P. and Solari, G. (2004), "Equivalent static wind actions on vertical structures", *J. Wind Eng. Ind. Aerod.*, **92**, 335-357.

Simiu, E. and Scanlan, R.H. (1996), *Wind Effects on Structures*, John Wiley and Sons, USA.

Solari, G. (1982), "Alongwind response estimation: closed form solution", *J. Struct. Div. ASCE*, **108**(1), 225-244.

Solari, G. and Carassale, L. (2000), "Modal transformation tools in structural dynamics and wind engineering", *Wind Struct.*, **3**(4), 221-241.

Solari, G. and Piccardo, G. (2001), "Probabilistic 3-D turbulence modeling for gust buffeting of structures", *Probabilistic Eng. Mech.*, **16**, 73-86.

Solari, G. and Tubino, F. (2005), "Gust buffeting of long-span bridges by Double Modal Transformation", *Proc. of the Fourth European & African Conf. on Wind Engineering*, Prague, July.

Tubino, F. and Solari, G. (2007), "Gust buffeting of long span bridges: Double Modal Transformation and effective turbulence", *Eng. Struct.*, **29**(8), 1698-1707.

UNI EN 1991-1-4 (2005), *Actions on structures - Parte 1-4: General actions - Wind actions*, Eurocode 1.

Appendix

The linearised equation of motion of the bridge deck in the x direction is given by:

$$\left(E_T J_T + \frac{E_T J_{xy} C_V^2(z)}{h_P^2}\right)\frac{\partial^4 x(z,t)}{\partial z^4} + \frac{4E_T J_{xy}}{h_P^2} C_V(z)\frac{\partial C_V(z)}{\partial z}\frac{\partial^3 x(z,t)}{\partial z^3} - N_T^{(\circ)}(z)\frac{\partial^2 x(z,t)}{\partial z^2}$$

$$-\frac{\partial N_T^{(\circ)}(z)}{\partial z}\frac{\partial x(z,t)}{\partial z} + \left\{\frac{2}{3}\frac{\gamma_C}{g}a_C s_C^{(\circ)}(z)\left[1+\left(\frac{C_V(z)B}{2h_P}\right)^2\right] + m_T\left[1+\left(\frac{C_V(z)B^2}{4h_P^2}\right)\right]\right\}\frac{\partial^2 x(z,t)}{\partial t^2}$$

$$+\left\{\frac{2}{3}\xi_C c_{cC} s_C^{(\circ)}(z)\left[1+\left(\frac{C_V(z)B}{2h_P}\right)^2\right] + \xi_T c_{cT}\left[1+\left(\frac{C_V(z)B^2}{4h_P^2}\right)\right] + \rho\bar{u}Bc_D\right\}\frac{\partial x(z,t)}{\partial t}$$

$$+\left\{\frac{1}{2}B^2 C_E(z)(1-C_V(z))^2 + \frac{g_T}{h_P}\left[1+\left(\frac{C_V(z)B}{2h_P}\right)^2\right]\right\}x(z,t) = \frac{1}{2}\rho\bar{u}^2 Bc_D + \rho\bar{u}\sigma_u u'(z,t)Bc_D$$

with:

$$C_E(z) = \frac{E_C(z)a_C}{(s_C^{(\circ)}(z))^3};\quad E_C(z) = E_S\Big/\left\{1+\frac{\gamma_C^2[(z-l_1)^2+(B/2)^2]E_S}{12[\sigma_C^{(\circ)}(z)]^3}\right\};\quad \sigma_C^{(\circ)}(z) = \frac{S_C^{(\circ)}(z)\Delta z}{A_C};$$

$$S_C^{(\circ)}(z) = \frac{g_T s_C^{(\circ)}(z)}{2h_P};\quad N_T^{(\circ)}(z) = -T_{CA}^{(\circ)} - \frac{g_T}{2h_P}[2l_1 z - z^2]\quad z\in[0,l_1];$$

$$N_T^{(\circ)}(z) = -\frac{g_T}{2h_P}[L_T^2 - 2L_T l_1 - z^2 + 2zl_1]\quad z\in[l_1,L_T];$$

$$T_{CA}^{(\circ)} = \frac{2E_{CA}A_{CA}l_1^2H_P^3}{3E_P J_P s_{CA}^{(\circ)^3} + 2E_{CA}A_{CA}l_1^2H_P^3}\left\{\frac{g_T}{2h_P}[L_T^2 - 2L_T l_1]\right\};\quad E_{CA} = E_S\Big/\left\{1+\frac{\gamma_C^2[4l_1^2+B^2]E_S}{48\,\sigma_{CA}^{(\circ)^3}}\right\};$$

$$s_{CA}^{(\circ)} = \sqrt{(B/2)^2 + h_P^2 + l_1^2};\quad E_S = E_T;\quad J_{xy} = J_{Tx}B^2/4;\quad c_{cT} = 2m_T\omega_x;\quad c_{cC} = 2\omega_x a_C\gamma_C/g.$$

The function $C_E(z)$ has been linearised (Monaco and Fiore 2005). The numerical applications have been carried out considering the data reported in Table 5. Moreover the value $\sigma_{CA}^{(\circ)}$ = 43.2 kN/cm^2 has been assumed.

Table 5 Data of the cable-stayed bridge used for the numerical applications

A_{CA} = 0.0346 (m^2)	A_C = 0.0113 (m^2)	E_T = 21000 (kN/cm^2)	E_P = 3122 (kN/cm^2)
J_{Tx} = 0.36 (m^4)	J_P = 112.26 (m^4)	J_T = 10 (m^4)	g_T = 193.11 (kN/m)